Available online at www.sciencedirect.com
SCIENCE DIRECT®
International Journal of Solids and Structures 43 (2006) 206–221
INTERNATIONAL JOURNAL OF SOLIDS and STRUCTURES
www.elsevier.com/locate/ijsolstr

Multiscale constitutive modeling and numerical simulation of fabric material

Ben Nadler, Panayiotis Papadopoulos *, David J. Steigmann

Department of Mechanical Engineering, University of California, Berkeley, 6131 Etcheverry Hall, CA 94720-1740, USA

Received 19 August 2004; received in revised form 18 May 2005
Available online 11 July 2005

Abstract

A multiscale model for a fabric material is introduced. The model is based on the assumption that on the macroscale the fabric behaves as a continuum membrane, while on the microscale the properties of the microstructure are accounted for by a constitutive law derived by modeling a pair of overlapping crimped yarns as extensible elasticae. A two-scale finite element method is devised to solve selected boundary-value problems.

Keywords: Fabric; Multiscale; Microstructure; Elastica; Finite element

1. Introduction

Fabric materials find numerous important applications ranging from lightweight ballistic shields (e.g., body armor, aircraft fuselage barriers) to high-strength flexible systems (e.g., parachutes) to everyday clothing manufacture. In recent years, many cutting-edge applications have focused on certain special-purpose fabric materials like Kevlar® and Zylon® that have extremely high strength-to-weight ratio. These materials are becoming mainstays in ballistic impact and penetration (see e.g., Laible, 1980; Cunniff, 1992; Adanur, 1995, Section 11), hence the accurate modeling of their mechanical response is increasingly important.

The material properties of fabric are greatly affected by their underlying microstructure. Fabric is made of yarns which are woven in one of several different patterns. Each yarn, in turn, is comprised of many thin fibers which are bundled together into a single structure. Adopting a largely macroscopic view, fabric may be modeled as a homogeneous material, as in Taylor and Vinson (1990). On the other hand, in Shim et al.

* Corresponding author. Tel.: +1 5106423358; fax: +1 5106426163.
E-mail address: panos@me.berkeley.edu (P. Papadopoulos).

0020-7683/$ - see front matter © 2005 Published by Elsevier Ltd.
doi:10.1016/j.ijsolstr.2005.05.020

(1995) fabric is modeled as a network of pin-jointed flexible truss elements. A more refined consideration of the microstructure is included in Ting et al. (1998), where the yarns are modeled as piecewise straight rigid rods joined by torsional springs and connected to overlapping yarns by linear springs. Likewise, in Tabiei and Ivanov (2002) a continuum-like membrane model is employed in which the in-plane stiffness is determined by a homogenization method applied over all yarns comprising the fabric. The alternative route of fully resolving (as opposed to modeling) the microstructure is explored in Shockey et al. (1999), where, however, the prohibitive cost of such an analysis for practical engineering designs is noted.

In this study, fabric is modeled using a multiscale approach. At the continuum level, the material behaves as a finitely deformable membrane. At the fine scale, the microstructure of the fabric is modeled by way of a pair of initially curved overlapping orthogonal elasticae under periodic boundary conditions subject to the constraint of non-penetration, as originally suggested in Warren (1990). In this manner, the fine scale is governed by two ordinary differential equations subject to a scalar integral constraint equation. A handshake process is developed to couple the two levels of analysis. Making use of this process, a robust finite element-based algorithm is formulated and implemented.

The organization of this paper is as follows: Section 2 describes in detail the proposed multiscale model of fabric. The numerical implementation is discussed in Section 3 and is followed by representative numerical simulations in Section 4.

2. Multiscale fabric model

In this section, the basic assumptions regarding the two-scale modeling of fabric materials are presented and discussed.

2.1. Macroscopic scale

On the macroscale, the current configuration of the fabric is represented by a smooth, oriented surface σ embedded in the three-dimensional Euclidean point-space $\mathscr{E}^3$. Given its smoothness, the surface possesses at each point a unique unit normal vector $\mathbf{n}$ and associated tangent plane $T\sigma$. In addition, two unit vector fields $\mathbf{l}_\alpha$, $\alpha = 1,2$, on $T\sigma$ are aligned with the directions of the overlapping yarns (see Fig. 1). For simplicity, the yarns are taken to be orthogonal in the reference configuration Σ of the surface along the directions of the unit vectors $\mathbf{L}_\alpha$, $\alpha = 1,2$. It follows that the surface deformation gradient in the macroscale can be expressed as

$$\mathbf{F} = \lambda_1 \mathbf{l}_1 \otimes \mathbf{L}_1 + \lambda_2 \mathbf{l}_2 \otimes \mathbf{L}_2, \tag{1}$$

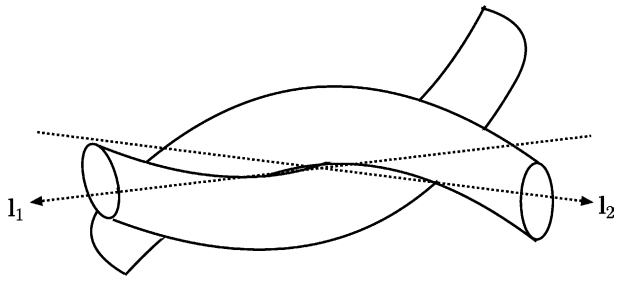

Fig. 1. Alignment of unit vectors $\mathbf{l}_\alpha$, $\alpha = 1, 2$, with the yarns in the current configuration.

where λ_α, $\alpha = 1, 2$, are the material stretches along the two yarn directions (see Nadler and Steigmann, 2003). Similarly, the two-dimensional Jacobian is defined as $J = [\det(\mathbf{F}^{\mathrm{T}}\mathbf{F})]^{1/2}$ and the two-dimensional Lagrangian strain takes the form

$$\mathbf{E} = \frac{1}{2}[(\lambda_1^2 - 1)\mathbf{L}_1 \otimes \mathbf{L}_1 + (\lambda_2^2 - 1)\mathbf{L}_2 \otimes \mathbf{L}_2 + \lambda_1\lambda_2(\mathbf{l}_1 \cdot \mathbf{l}_2)(\mathbf{L}_1 \otimes \mathbf{L}_2 + \mathbf{L}_2 \otimes \mathbf{L}_1)]. \tag{2}$$

By convention, the index values $\alpha = 1$ and 2 correspond to the so-called warp and fill (weft) directions, respectively (see e.g., Adanur, 1995, Section 4.4 for background on fabric weaving). This distinction becomes important when differentiating the response of the fabric based on the alignment of its yarns.

The referential statement of linear momentum balance is written in local form as

$$\mathrm{Div}\mathbf{P} + J\mathbf{f} = \rho\dot{\mathbf{v}}, \tag{3}$$

where Div is the referential two-dimensional divergence operator, $\mathbf{P}$ is the two-dimensional first Piola–Kirchhoff stress tensor, and $\mathbf{f}$ is the surface force per unit area (see again Nadler and Steigmann, 2003). The surface force $\mathbf{f}$ is due to applied tractions or two-dimensional counterparts of body forces (e.g., gravity). A constitutive equation for the stress tensor $\mathbf{P}$ is derived from fine scale considerations in the subsequent section.

2.2. Fine scale

This section describes a model consisting of a pair of overlapping yarns. This model forms the basis for the fine scale analysis of the fabric material. The fine-scale elastic model is used solely to determine the macroscale constitutive response.

2.2.1. Yarn model

Following earlier work in Warren (1990), each yarn is modeled on the fine scale as an extensible elastica under quasi-static loading, see also an earlier work on slender filaments by Buckley et al. (1980). The equation of equilibrium for the in-plane bending of an elastica takes the form (see e.g., Antman, 1968)

$$\frac{\mathrm{d}}{\mathrm{d}S}\left[B\frac{\mathrm{d}}{\mathrm{d}S}[\phi(S) - \Phi(S)]\right]\left(1 + \frac{N(S)}{A}\right)^{-1} = -Q(S), \tag{4}$$

In the preceding equation, N and Q denote the internal tensile and shearing forces, respectively. Also, ϕ and Φ stand for the yarn angle in the current and in the (stress-free) reference configuration of the yarn, respectively. All these variables are parametrized by the referential arc-length S of the elastica. Furthermore, A and B are the stretching and bending stiffness of the yarn, respectively, which are taken to be constants. The elasticae associated with each yarn are assumed to deform solely due to mixed Dirichlet–Neumann boundary conditions applied at their end points. These conditions are derived from geometric considerations in Section 2.3. In general, the values of A and B, as well as the function $\Phi(S)$ are dependent on the particular yarn type and can be determined by experimental means.

2.2.2. The unit cell in the fine scale

This section describes in detail the unit cell of the fine scale. Given any point p on the membrane σ, the unit cell C_p consists of two overlapping, initially curved and planar elasticae representing the two sets of yarns. The point p is defined to be the projection on σ of the point of contact between the two elasticae, as seen in Fig. 2 for the reference configuration. Each planar elastica is further assumed to be homogeneous within the cell and symmetric with respect to the plane that passes through the contact point and is orthogonal to the yarn. It follows that the projection of the unit cell C_p on the tangent plane $T_p\Sigma$ in the reference configuration is a rectangle centered at p and whose sides have length equal to the projections of the half-period of the

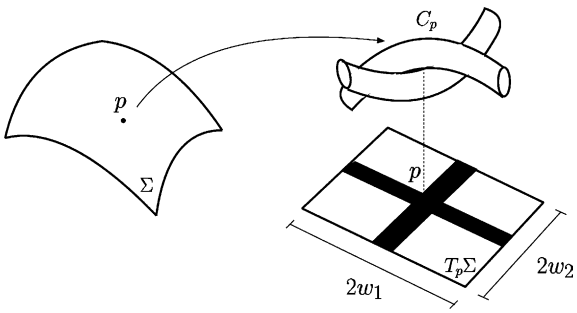

Fig. 2. A schematic representation of the multiscale modeling for fabric in the reference configuration.

weaving of each of the overlapping yarns (see again Fig. 2). In summary, the salient kinematic assumptions in the fine scale are as follows:

(i) The yarns are initially orthogonal.
(ii) Stretching of the two yarns occurs symmetrically with respect to the midpoint (also, contact point, when contact occurs) of the yarns.

Each yarn in the unit cell C_p is subject to equal and opposite end-point displacements in the direction defined by the intersection of the tangent plane $T_p\sigma$ with the plane of the yarn. These displacements give rise to corresponding reaction forces F_α which are transmitted to the macroscopic problem as part of the handshake process discussed in Section 2.3. Also, the constraint of non-penetration gives rise to an internal force V between the two yarns that acts as a Lagrange multiplier at the point of contact. Since the stretching of the two yarns occurs symmetrically with respect to their contact point, sliding is suppressed and the internal force V is normal to the tangent plane $T_p\sigma$, as in Fig. 3.

The preceding kinematic assumptions for the yarn model are fully consistent with the macroscale membrane model. Indeed, it is emphasized here that the fine-scale elastica boundary-value problem is used solely to determine the macroscale *constitutive* response. Given that shear *resistance* of the yarns is neglected in the macroscale (although shear deformation *is* allowed), the macroscale constitutive behavior is fully determined by the model under the preceding assumptions. Thus, for the purpose of determining *constitutive* response alone in a manner consistent with the macroscale assumptions, the restriction to orthogonality of the yarns may be made without loss of generality.

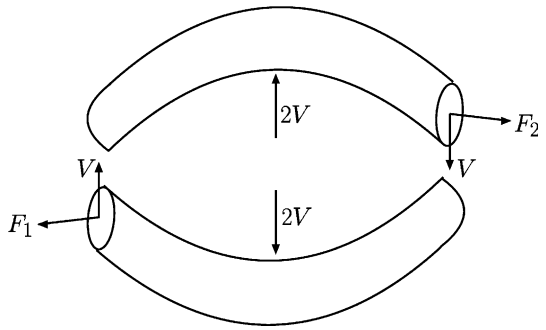

Fig. 3. Detail of the internal force V and external forces F_1 and F_2 acting on the unit cell (for clarity, the two yarns are depicted as detached from each other).

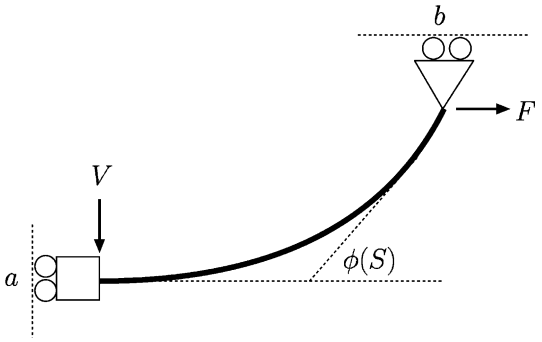

Fig. 4. Boundary-value problem for a yarn.

It follows from the symmetry of the yarn configuration and applied loading that one needs to analyze the fine-scale problem only for one quarter of the unit cell that includes one-half of each yarn, as in Fig. 4. For the elastica under consideration in a state of equilibrium, the internal tension and shear are related to the forces F_α and V by

$$N_\alpha(S) = F_\alpha \cos\phi_\alpha(S) + V \sin\phi_\alpha(S), \quad Q_\alpha(S) = -F_\alpha \sin\phi_\alpha(S) + V\cos\phi_\alpha(S). \tag{5}$$

To formulate appropriate boundary conditions, let L_α be the length of the half-period of the elastica corresponding to yarn α. Then, taking $S = 0$ to be the point of contact, the boundary conditions for the elasticae take the form

$$\phi_\alpha(0) = 0, \quad \frac{\mathrm{d}}{\mathrm{d}S}(\phi_\alpha(S) - \Phi_\alpha(S))\Big|_{S=L_\alpha} = 0. \tag{6}$$

Condition $(6)_1$ is a statement of symmetry of the deformation with respect to the contact point. Condition $(6)_2$ reflects the requirement that the end points of the elasticae lie on the tangent plane $T_p\sigma$ and can sustain no moments, as is the case with membranes (see Fig. 5). The latter can be also understood as a periodic boundary condition.

The motions of the two elasticae are coupled through the constraint of non-penetration. To formulate this constraint, the displacement v_α of the contact point for yarn α relative to its end points is expressed as

$$v_\alpha = \int_0^{L_\alpha} \left[\left(1 + \frac{N_\alpha(S)}{A_\alpha}\right)\sin\phi_\alpha(S) - \sin\phi_\alpha^0(S)\right]\mathrm{d}S, \tag{7}$$

where ϕ_α^0 describes the yarn configuration when the fabric is macroscopically stress-free.[1] Note that, due to symmetry, the displacement v_α is necessarily in the direction of the normal to the tangent plane $T_p\sigma$ (see Fig. 4). A relative displacement d of the contact points of the two yarns can now be defined as

$$d = v_1 + v_2. \tag{8}$$

Clearly, the non-penetration condition is of an inequality type and incorporates two separate cases:

(a) The elasticae are in contact, hence the distance function d vanishes. This condition furnishes an equation to compute the value of the force $V(\geqslant 0)$.
(b) The elasticas separate, hence the distance function d becomes positive and the internal force V vanishes.

[1] The yarn configurations corresponding to Φ_α and ϕ_α^0 do not necessarily have to coincide.

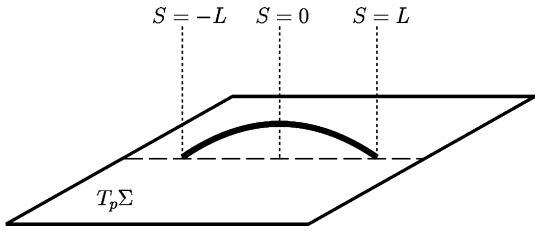

Fig. 5. The placement of a typical elastica relative to the tangent plane.

These two conditions can be expressed in the classical inequality constraint form

$$Vd = 0, \quad V \geqslant 0, \quad d \leqslant 0. \tag{9}$$

Given (8), (9) and the definition of the normal displacements in (7), it follows that the non-penetration constraint condition is expressed in integral form. The enforcement of this condition is discussed in Section 3.

The preceding fine-scale model relies on constitutive parameters both at the level of the single yarn and the weaving. On the single-yarn level, the parameters are the stretching stiffness A_α and bending stiffness B_α, as well as the stress-free shape $\Phi(S)$. All these quantities may be different for each of the two sets of yarns and are generally functions of position in the macroscopic sense. On the weaving level, the relevant property is the initial woven yarn shape ϕ^0_α, which controls the frequency (therefore also the unit cell size) and the amplitude of the weave.

2.3. Handshake process

This section describes the coupling (handshake) of the macroscopic and fine-scale problems. The basic structure of the coupling is as follows: the kinematics of the macroscopic scale is used as input to generate the forces in the fine scale. These forces, in turn, are used to define the stresses on the macroscopic scale.

The communication of kinematic information from the macroscopic to the fine scale requires the introduction of one or more characteristic lengths. In this problem, the natural lengths are the dimensions $2w_1$ and $2w_2$ of the unit cell in the reference configuration, as projected onto the tangent plane $T_p\Sigma$ (see Fig. 2). Clearly, these can be derived from the fabric stress-free yarn configuration ϕ^0_α as

$$w_\alpha = \int_0^{L_\alpha} \cos\phi^0_\alpha(S)\mathrm{d}S. \tag{10}$$

Further, recall that the displacements u_α of the end points of each elasticae relative to the corresponding symmetry points are given by

$$u_\alpha = \int_0^{L_\alpha} \left[\left(1 + \frac{N_\alpha(S)}{A_\alpha}\right)\cos\phi_\alpha(S) - \cos\phi^0_\alpha(S)\right]\mathrm{d}S. \tag{11}$$

Observe that, owing again to the assumption that the end point of the elasticae lie always on $T_p\sigma$, the displacements u_α are along the directions defined by the intersection of the elasticae with $T_p\sigma$. Kinematic coupling between the two scales is effected by the relation

$$u_\alpha = (\sqrt{1+2E_\alpha} - 1)w_\alpha, \quad E_\alpha = \mathbf{L}_\alpha \cdot \mathbf{E}\mathbf{L}_\alpha \quad (\text{no sum over } \alpha). \tag{12}$$

This relation is derived by assuming that the macroscopic stretch $\lambda_\alpha = \sqrt{1+2E_\alpha}$ gives rise to a fine-scale displacement u_α through its uniform application over the length w_α.

The fine scale problem of two overlapping elasticae produces end-point reaction forces F_α in the direction of the yarns on $T_p\sigma$. This implies that the first Piola–Kirchhoff stress of the macroscopic scale is of the special form

$$\mathbf{P} = P_1\mathbf{l}_1 \otimes \mathbf{L}_1 + P_2\mathbf{l}_2 \otimes \mathbf{L}_2. \tag{13}$$

where P_α is the force acting along $\mathbf{l}_\alpha$ per unit reference length in the direction transverse to $\mathbf{L}_\alpha$ (see Nadler and Steigmann, 2003). In general, the stress P_α can be tensile or compressive, depending on the imposed stretch. However, compressive stresses lead to ill-posedness of the membrane problem, hence do not play a prominent role here. The force F_α and the stress P_α are related by

$$P_1 = \xi_2 F_1, \quad P_2 = \xi_1 F_2, \tag{14}$$

where ξ_α $(= \frac{1}{2w_\alpha})$ is the α-yarn density in the reference configuration, i.e., the number of α-yarns per unit length in the direction normal to $\mathbf{L}_\alpha$ on Σ. Likewise, the internal force V in the fine scale translates to internal pressure P_0 (i.e., force per unit referential area) in the membrane, according to

$$P_0 = \xi_1\xi_2 V, \tag{15}$$

where the product $\xi_1\xi_2$ is the overlapping area density in the reference configuration.

In summary, the macroscopic balance laws (3) and the fine-scale equilibrium equation (4), subject to (6), (5) and (9), comprise the governing system of equations for the multiscale analysis of fabric materials. Eqs. (10)–(14) establish the relationship between the two scales. Notice that balance of angular momentum on the macroscale is satisfied automatically when the deformation gradient and the first Piola–Kirchhoff stress are given by (1) and (13), respectively.

3. Algorithmic formulation

A solution to the multiscale problem described in Sections 2.1 and 2.2 is obtained using a two-level finite element formulation supplemented by a numerical counterpart of the handshake process of Section 2.3.

The balance laws (3) of the macroscopic model are satisfied weakly by way of a standard Galerkin-based finite element formulation of a finitely deforming membrane, whose stress response is governed by the fine-scale model. The solution of the equilibrium Eq. (4) for each of the two elasticae in the fine-scale model is also obtained using Galerkin-based finite elements, subject to conditions (9). Closure to the fine-scale problem is provided by the handshaking process through condition (12), which may be recast using (10) and (11) in the form

$$\sqrt{1+2E_\alpha}\int_0^{L_\alpha} \cos\Phi_\alpha(S)\mathrm{d}S = \int_0^{L_\alpha}\left[\left(1+\frac{N_\alpha(S)}{A_\alpha}\right)\cos\phi_\alpha(S)\right]\mathrm{d}S \quad (\text{no sum over } \alpha). \tag{16}$$

The integral equations (16) are reduced to algebraic approximants using the quadrature rules (here, Gauss-type) applied elementwise to the Galerkin terms. A standard dual method is employed for the resulting discrete inequality-constrained problem. This leads to a system of nonlinear algebraic equations which includes the weak forms of the elastica equilibrium, the boundary conditions (16) and the non-penetration constraint. This system is solved monolithically for the angles ϕ_α, the end-point forces F_α, and the Lagrange multiplier V. In particular, a predictor–corrector scheme is implemented whereby the constraint is assumed to hold initially in equality form. If the resulting force V turns out to be negative (i.e., adhesive), the governing equations are resolved with the equality constraint condition deactivated. The Newton–Raphson method is employed to solved the nonlinear algebraic system for the fine-scale model. As in other dual formulations, the resulting generalized stiffness matrix is symmetric and its profile is narrow, with the exception of the row/column associated with the constraint equation. A standard direct method is used for the solution of this system.

The macroscopic problem is solved using an inexact Newton–Raphson method in which the geometric stiffness of the membrane is determined without any approximation, while an estimate of the material stiffness is derived using a numerical technique. Specifically, the latter is calculated by first incrementing each of the macroscale strains E_α by ΔE_α, while holding the other fixed, then computing the two sets of forces P_α and $P_\alpha + \Delta P_\alpha$ for both yarns, and finally using a secant approximation to the material tangent modulus. This (generally unsymmetric) material tangent modulus is subsequently used in the material tangent stiffness of the macroscopic problem. Recall that symmetry of the material tangent stiffness matrix is generally due to the fact that it is derived from a potential. However, such a potential is not introduced in this case, which leads to the unsymmetry.

It should be emphasized that in the proposed multiscale model, the size of the finite element mesh used for the membrane discretization is independent of the size of the unit cell. Hence, it is straightforward to perform adaptive mesh refinement in order to resolve high macroscopic-scale strain gradients due to, e.g., impact loading. Of course, to respect the separation of scales, the membrane mesh size should be appropriately larger than the unit cell size.

4. Numerical results

The multiscale model has been implemented in FEAP, a general-purpose finite element program partially documented in Zienkiewicz and Taylor (2000). The macroscopic model is discretized using 4-node displacement-based quadrilateral membrane elements with full (2×2) integration. The fine-scale model is discretized using 2-node element with the nodal values of ϕ_α as unknowns. The fine-scale problem is formulated and solved at each Gauss point of the membrane, as discussed in Section 3.

4.1. Stress–strain relations

A set of homogeneous deformations is applied to the fabric in order to assess its macroscopic stress–strain response, as well as the dependence of the constraint force V on the loading. Here, the material parameters for the fine-scale model are taken to be

Yarn	A_α [N]	B_α [N/mm^2]	L_α [mm]	$\phi^0_\alpha(L_\alpha)$ [rad]
Warp ($\alpha = 1$)	1156	0.027975	0.2444	0.3251
Fill ($\alpha = 2$)	1165	0.045668	0.2416	0.1368

The preceding values of the material parameters correspond to Kevlar® 29 and are adapted from Ericksen et al. (1992). Notice that the two sets of yarns (warp and fill) have different material and geometric properties. Here, it is assumed that the yarn configuration corresponding to stress-free fabric is approximated by a smooth curve defined by the function

$$\phi^0_\alpha(S) = \phi^0_\alpha(L_\alpha)\sin\left(\frac{\pi S}{2L_\alpha}\right). \tag{17}$$

Unlike the circular arc employed in Ericksen et al. (1992), this choice guarantees that the curvature, and hence the bending moment, vanishes at the end points of the unit cell. It is further assumed that the stress-free configuration of the yarns coincides with the configuration corresponding to stress-free fabric, namely that $\Phi_\alpha(S) = \phi^0_\alpha(S)$. Taking into account Eqs. (10) and (17), and the preceding values of the geometric properties, the yarn densities are computed to be $\xi_1 = 2.10$ yarns/mm and $\xi_2 = 2.08$ yarns/mm.

In the following figures, it is assumed that the material is strained homogeneously along the yarn directions. Figs. 6 and 7 depict, respectively, the stress P_1 in the warp direction and the internal stress

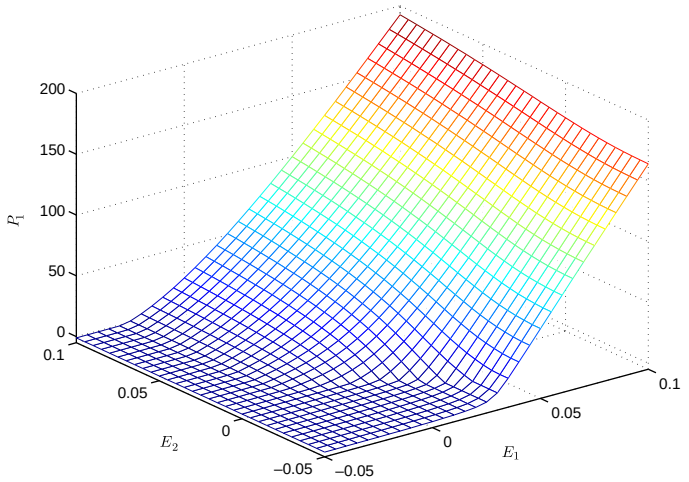

Fig. 6. Homogeneous biaxial deformation: stress P_1 [N/mm] vs strains E_1 and E_2.

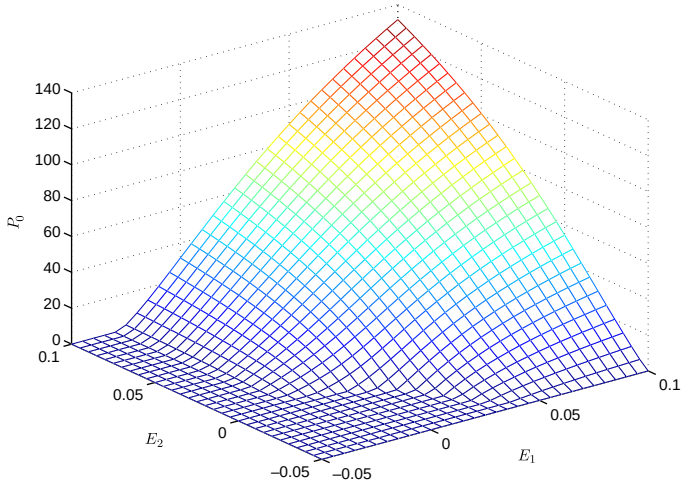

Fig. 7. Homogeneous biaxial deformation: internal stress P_0 [N/mm^2] vs strains E_1 and E_2.

P_0 as functions of biaxial Lagrangian strain effected via displacement control. Notice that P_1 is negligible for values of (E_1, E_2) that correspond to separation of the yarns (i.e., where P_0 vanishes). For any constant value of E_2, the stress P_1 increases upon contact between the two yarns. This increase is becoming sharper with decreasing values of E_2. This is because lower values of E_2 permit a greater amount of decrimping for the warp yarns before contact is established. Also note that the distribution of P_0 in Fig. 7 is not symmetric, reflecting the asymmetry of warp and fill yarns.

Figs. 8–10 illustrate the fine-scale behavior of the fabric under uniaxial extension and compression in the warp direction. Fig. 8 shows that the stress P_1 is very small in the compressive range. The same stress remains very small in the initial stage of extension, as the warp yarns decrimp without meeting any significant resistance from the fill yarns; note the small values of the internal stress in Fig. 10. Despite the small stresses, it is emphasized that the transition to contact is non-smooth, as evident from the detail plot in Fig. 8.

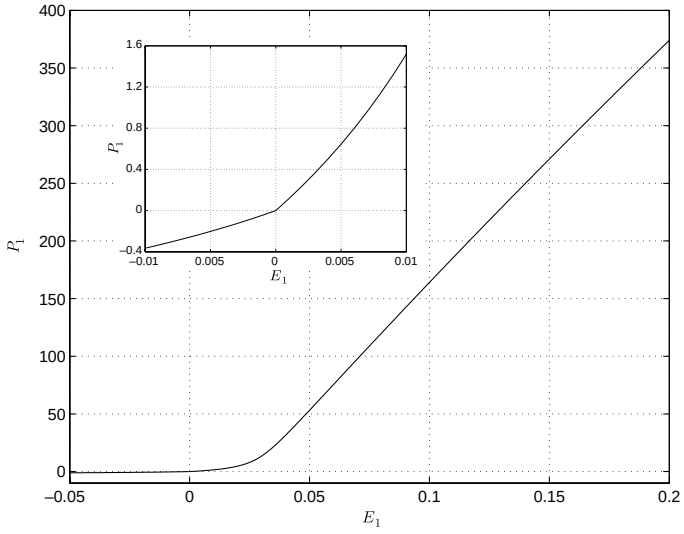

Fig. 8. Homogeneous uniaxial deformation: stress P_1 [N/mm] vs strain E_1 for $P_2 = 0$.

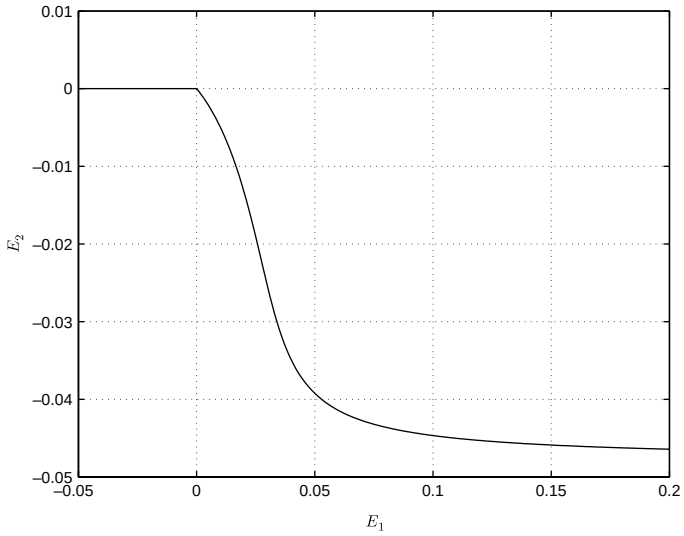

Fig. 9. Homogeneous uniaxial deformation: E_2 vs E_1 for $P_2 = 0$.

Once decrimping reaches an advanced stage, P_1 starts increasing rapidly due to the tensile stiffness of the (nearly straight) warp yarns. Fig. 9 demonstrates that decrimping of the warp yarns in uniaxial extension necessitates crimping of the fill yarns in order for the non-penetration constraint to be satisfied. This leads to a Poisson-like effect in the macroscopic scale. In particular, the sharp decrease of E_2 is due to the decrimping of the warp yarns. Again, once the decrimping is advanced, E_2 is reduced more slowly and ultimately asymptotes to a constant value. An analogous behavior is depicted in Fig. 10, where the internal stress is shown to rise sharply upon contact due to decrimping of the warp yarns. The stress P_0 asymptotes to a maximum value as the decrimping is completed.

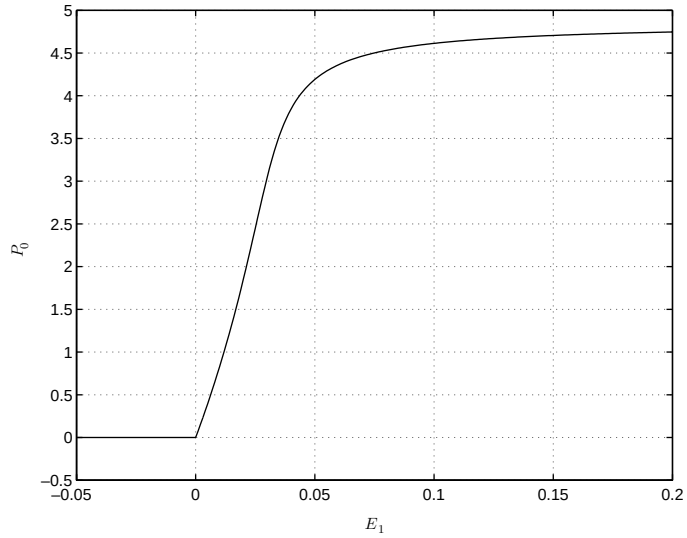

Fig. 10. Homogeneous uniaxial deformation: internal stress P_0 [N/mm^2] vs E_1 for $P_2 = 0$.

4.2. Poking of a fabric sheet

A flat square sheet of fabric is deformed quasi-statically by displacing its geometric center normal to the fabric plane, while its boundary is kept fixed. The sides of the sheet have length $a = 100$ mm. Fig. 11 illustrates the dependence of the reaction force at the point of loading on the imposed displacement. The response in these two measures is consistent with that of a normal membrane. Fig. 12 shows the

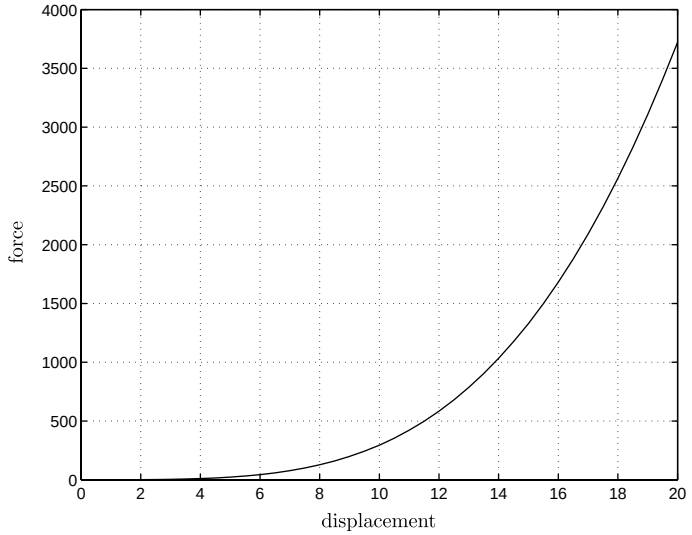

Fig. 11. Poking of a fabric sheet: reaction force in [N] vs displacement in [mm] at geometric center.

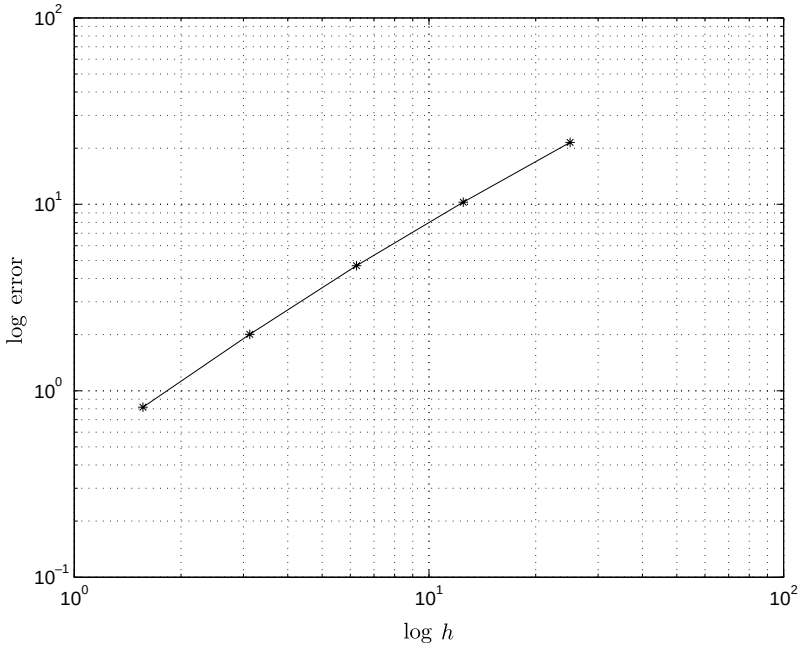

Fig. 12. Poking of a fabric sheet: convergence of the reaction force under uniform h-refinement.

convergence of the reaction force generated by a normal displacement of 5 mm under uniform h-refinement of the mesh. Also, the initial orientation of the fibers is taken to be parallel to the edges of the sheet.

It is instructive to compare the stress and strain distributions in this problem to the respective distributions for an "equivalent" isotropic, homogeneous nonlinearly elastic membrane. For this comparison to be meaningful, it is assumed that both sets of yarns have the geometric and material properties of the warp yarns in Section 4.1. The membrane is assumed to obey the Kirchhoff–St. Venant law in the second Piola–Kirchhoff stress and Lagrangian strain, with material parameters $\lambda = 1345$ MPa and $\mu = 407$ MPa. These parameters are estimated from the macroscopic tension and shear of the fabric sheet by considering the asymptotic response in Fig. 8 and the initial response in Fig. 9. Two special cases are considered: (a) the initial yarn directions are aligned with the edges of the sheet, and (b) the initial yarn directions form a 45°-angle with the edges of the sheet. Fig. 13 includes plots of the normal component of the second Piola–Kirchhoff stress and the Lagrangian strain in the direction of one of the edges for normal displacement of 5 mm imposed at the geometric center of the sheet. It is clear that the strain distribution of the fabric is very different than that of the membrane, although the imposed displacement is the same at the center point. Specifically, the Poisson-like effect in the fabric is localized and accentuated due to the channeling of strain along the yarns that directly sustain the load. Likewise, the stress distribution differs qualitatively in the two models. Indeed, in the case of the fabric, the stress is again localized in a small band aligned with the yarns. This, in fact, shows that the capacity of the fabric material to sustain loads (and, by extension, damage) is limited by this localized behavior. Fig. 13 also contains plots of the same stress and strain components when the initial yarn directions form an angle of 45° with the sheet edges. Here, the misalignment of the yarns with the sheet edges yields substantially different distributions due to the pronounced anisotropy of the material.

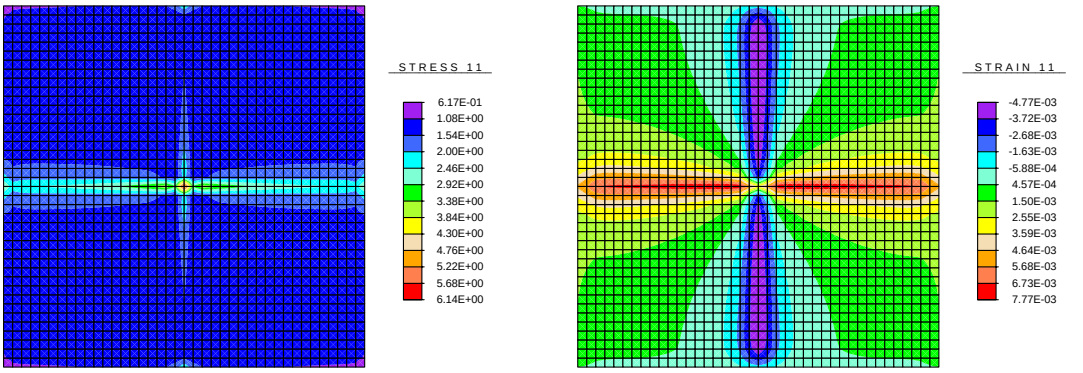

(i) Fabric sheet with yarns aligned to the edges

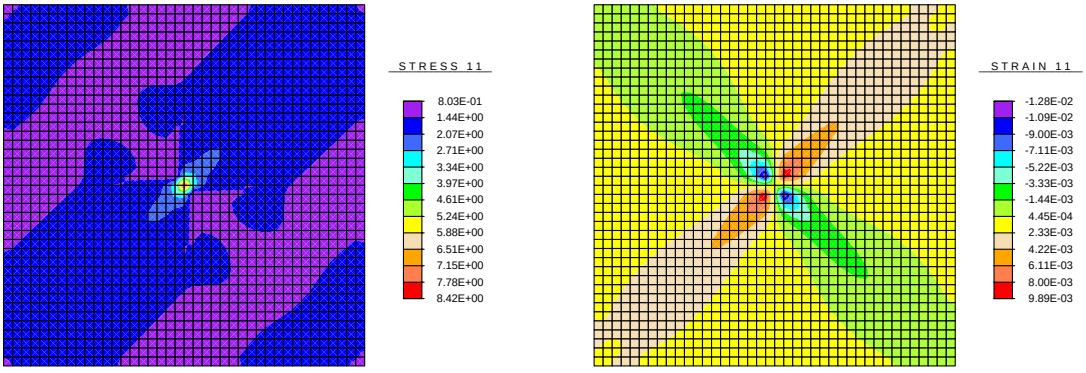

(ii) Fabric sheet forming a 45^o-angle to the edges

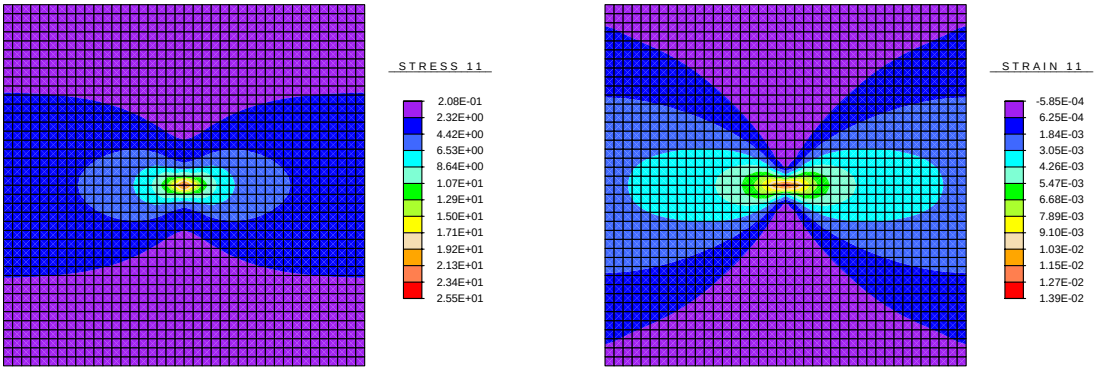

(iii) Elastic membrane

Fig. 13. Poking of a fabric sheet: Distributions of the normal component of the second Piola–Kirchhoff stress in N/mm and Lagrangian strain in the horizontal direction for fabric and for homogeneous isotropic membrane.

4.3. Push test on a fabric sheet

This simulation intends to model an experiment conducted on Zylon® (see Shockey et al., 2001). This experiment concerns the quasi-static contact of a rigid solid with a fabric sheet. The simulation uses the following values for kinematic and material parameters:

Yarn	A_α [N]	B_α [N/mm^2]	L_α [mm]	$\phi^0_\alpha(L_\alpha)$ [rad]
Warp ($\alpha = 1$)	5800	0.140	0.3672	0.2807
Fill ($\alpha = 2$)	6250	0.245	0.3622	0.1546

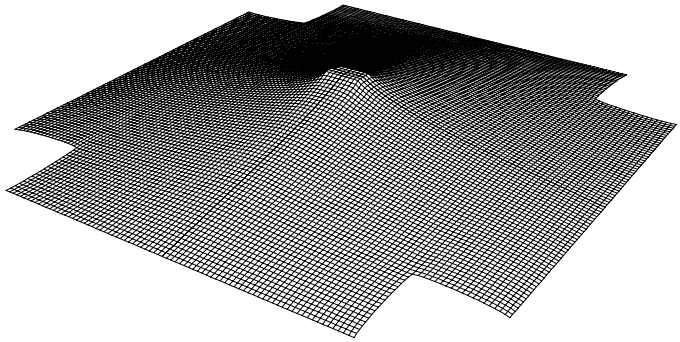

Fig. 14. Push test on a fabric sheet: Finite element mesh of the deformed configuration for maximum push (0.75 in).

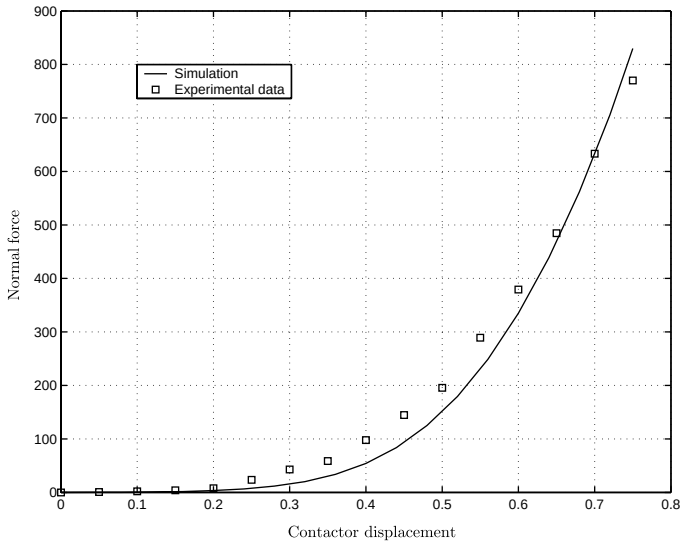

Fig. 15. Push test on a fabric sheet: Total normal force in lbs vs contactor displacement in inch for experiment and simulation.

In the preceding table, the values of A and L_α are taken directly from the cited report. The value of B (bending coefficient) is not listed in the report and it is here estimated by assuming the same ratio A/B as in Section 4.1. It is noted that due to the extremely low bending stiffness, the precise value of B does not substantially affect the answers. The value of $\phi_\alpha^0(L_\alpha)$ is estimated from the experimental data by taking the given values of L_α and w_α and assuming the initial yarn shape in (17). Notice that the sheet has the shape of a cross and it fully restrained at its four edges (Shockey et al., 2001, Figure 13). The sheet is doubly symmetric with a long dimension of 7.25 in and arm width of 5 in. In the experiments, the contactor is modeled as a rigid block with a tapered rectangular cross-section of dimension 0.5 in $\times$ 0.25 in. However, due to the magnitude of the taper angle the tapered portion is ignored in the simulation and flat and fixed bilateral contact conditions are enforced. In addition, the initial yarn directions align with the two arms of the cross, as in the experiments. The induced double symmetry allows for the meshing of only a quarter of the full domain.

Successive finite element analyses were conducted under uniformly increasing mesh refinement to ensure convergence of the solution. Fig. 14 depicts the deformed configuration of the sheet at maximum push (0.75 in). Also, Fig. 15 shows a good agreement between the experimental and the numerical results. The small disparity may be attributed to the assumed shape of the yarns and/or the potential non-linearity of the elastic law in the fine scale modeling.

5. Conclusions

The multiscale model of fabric proposed in this paper captures the salient anisotropic features of the material by directly modeling the yarns and their interaction as two overlapping elasticae. One of its major advantages over other models is that it includes an internal stress which will be used in subsequent work to incorporate the effects of friction between the yarns. In addition, the model is amenable to robust computational implementation and can be readily incorporated in a finite element environment.

Acknowledgement

The authors would like to acknowledge support by the Homer Powley Fund for Research in Small Arms Ballistics, administered by the Department of Mechanical Engineering at the University of California, Berkeley.

References

Adanur, S., 1995. Wellington Sears Handbook of Industrial Textiles. Technomic, Lancaster.

Antman, S., 1968. General solutions for plane extensible elasticae having nonlinear stress–strain laws. Q. Appl. Math. 26, 35–47.

Buckley, C., Lloyd, D., Konopasek, M., 1980. On the deformation of slender filaments with planar crimp: theory numerical solution and applications to tendon collagen and textile materials. Proc. R. Soc. Lond. A 372, 33–64.

Cunniff, P., 1992. An analysis of the system effects in woven fabrics under ballistic impact. Textile Res. J. 62 (9), 495–509.

Ericksen, R., Davis, A., Warren, W., 1992. Lightweight fragment barriers for commercial aircraft. Textile Res. J. 62 (11), 628–637.

Laible, R., 1980. Fibrous armor. In: Laible, R. (Ed.), Ballistic Materials and Penetration Mechanics. Elsevier, Amsterdam, pp. 73–115 (Chapter 4).

Nadler, B., Steigmann, D., 2003. A model for frictional slip in woven fabrics. Comptes Rendues: Mechanique 331, 797–804.

Shim, V., Tan, V.B., Tay, T., 1995. Modeling deformation and damage characteristics of woven fabric under small projectile impact. Int. J. Impact Engng. 16, 585–605.

Shockey, D., Erlich, D., Simons, J. 1999. Lightweight fragment barriers for commercial aircraft. Proceedings of 18th International Symposium on Ballistics, San Antonio, Texas, pp. 1192–1199.

Shockey, D., Erlich, D., Simons, J. 2001. Improved barriers to turbine engine fragments: Interim report III. Technical Report DOT/FAA/AR-99/8,III, SRI International.

Tabiei, A., Ivanov, I., 2002. Computational micro-mechanical model of flexible woven fabric for finite element impact simulation. Int. J. Numer. Meth. Engng. 153, 1259–1276.

Taylor, W., Vinson, J., 1990. Modeling ballistic impact into flexible materials. AIAA J. 28, 2098–2103.

Ting, C., Ting, J., Roylance, D., Cunniff, P. 1998. Numerical characterization of the effects of transverse yarn interaction on textile ballistic response. 30th International SAMPE Technical Conference, pp. 57–67.

Warren, W., 1990. The elastic properties of woven polymeric fabric. Polym. Engng. Sci. 30, 1309–1313.

Zienkiewicz, O, Taylor, R, 2000, fifth ed.The Finite Element Method, vols. 1–3 Butterworth-Heinemann, Oxford.